

5th US Combustion Meeting
Organized by the Western States Section of the Combustion Institute
and Hosted by the University of California at San Diego
March 25-28, 2007.

Microgravity Droplet Combustion in CO₂ Enriched Environments at Elevated Pressures

M. C. Hicks¹, V. Nayagam² and F. A. Williams³

¹*NASA Glenn Research Center, Cleveland, Ohio 44135, USA*

²*National Center for Space Exploration Research, Cleveland, Ohio 44135, USA*

³*Center for Energy Research, Department of Mechanical and Aerospace Engineering,
University of California at San Diego, La Jolla, California 92093-0411, USA*

Microgravity droplet combustion experiments were performed in elevated concentrations of CO₂ at pressures of 1.0 atm, 3.0 atm, and 5.0 atm to examine the effects of a radiatively participating suppression agent in space applications. Methanol and n-heptane droplets, with an initial diameter of 2.0 mm supported on a quartz fiber, were used in these experiments. The ambient O₂ concentration was held constant at 21% and the CO₂ concentrations ranged from 0% to a maximum of 70%, by volume with the balance consisting of N₂. Results from the methanol tests showed slight decreases in burning rates with increased CO₂ concentrations at all ambient pressures. The n-heptane tests show slight increases in burning rates with increasing CO₂ concentrations at each pressure level. Instantaneous radiative heat flux was also measured using both a broadband radiometer (i.e., wavelengths from 0.6 μm to 40.0 μm) and a narrowband radiometer (i.e., centered at 5.6 μm with a filter width at half maximum of 1.5 μm). Radiative exchanges between the droplet and surrounding gases as well as the soot field produce departures from the classical quasisteady theory which would predict a decrease in burning rates with increasing CO₂ concentrations in microgravity.

1. Introduction

It has long been recognized that radiative heat transfer can play an important role in the effectiveness of gaseous extinguishing agents in low-gravity environments. The radiative properties of the gas phase surrounding the fuel source may significantly alter Minimum Extinguishment Concentrations (MEC's) which are often used as an engineering criterion for fire suppression. The International Space Station currently employs CO₂ for the fire suppression system and a similar system remains a likely candidate for future extraterrestrial fire suppression systems because of its ready availability and ease of cleanup after discharge. However, CO₂ also has strong absorption bands in the infrared region of the electromagnetic spectrum and, as a consequence, may prove to be a less efficient suppression agent in space applications where radiative thermal losses play a significant role in flame quenching. If the gases surrounding a reduced-gravity flame absorb radiative energy then the increased temperatures of the surrounding gases, which are not convected away because of the absence of buoyant convection, will result in an increase in energy feedback to the fuel.

The effectiveness of CO₂ as a suppressant in space applications has been studied using a variety of flame configurations and numerical models. An opposed-flow configuration³ was used to compare

flame spread rates over solid fuels in the presence of different diluents [1]. In that study it was found, when comparing MEC's, that helium was a more effective suppressant than CO₂. In a numerical study using opposed jet-diffusion flames it was found that argon becomes more effective than CO₂ as a suppressant in low stretch-rate environments [2]. In a recent numerical study investigating cup-burner flames in zero gravity it was found that radiative losses become the dominant process in thermal quenching. In that study it was reported that the MEC for CO₂ increased by 32% compared to similar normal-gravity flames [3].

In contrast to those results, recent work investigating methanol droplets burning at elevated CO₂ concentrations with a constant volume fraction of 21% O₂ showed little change in the ratio of the radiative heat loss to the total heat release [4]. Here it was suggested that because of the small length scales associated with the 2 mm fuel droplets the increased radiative emissions from the radiating volume of CO₂ and product species were largely offset by decreases in flame temperature resulting from the higher effective specific heat of the gas mixture. More recently, results from a series of normal gravity experiments investigating n-heptane droplets in elevated concentrations of CO₂ in 21% O₂ have been reported [5]. This work showed a dramatic decrease in soot formation in the presence of CO₂ and an initial decrease in radiative emissions up to the point when soot was no longer present at which point radiative emissions began to increase.

A series of experiments designed to isolate the effects of the interaction between a radiatively participating suppression agent and a low-gravity flame have been performed. In addition to elevating ambient CO₂ concentrations, experiments have been performed at elevated pressures, effectively varying radiative length scales, and with both non-sooting and sooting fuels (i.e., methanol and n-heptane). These experiments serve as a follow-on to earlier work [4] and are a precursor to future suppressant flight experiments planned for the International Space Station.

2. Experimental Procedure

Experiments were conducted using experimental hardware and approaches similar to that already reported in earlier work [4, 6] and only an overview is presented here. All tests were performed in the NASA Glenn Research Center's *Zero Gravity Facility* (ZGF) allowing a microgravity duration of approximately 5.0 seconds. Droplets of either methanol or n-heptane were suspended on a 110 μm quartz fiber. Initial droplet diameters were $2.0 \text{ mm} \pm 0.15 \text{ mm}$ for the n-heptane droplets and were $2.0 \text{ mm} \pm 0.20 \text{ mm}$ for the methanol droplets. Ignition was accomplished with a hot-wire igniter made using 29 gauge Kanthal wire and this was placed approximately 1.0 mm from the droplet surface. The igniter was energized by a constant current of 4.3 amps for 1.6 seconds, after which it was retracted from the flame zone by actuation of a rotary solenoid. Diagnostics consisted of a wide-band radiometer (i.e., wavelengths ranging from 0.6 μm to 40 μm) and a narrow-band radiometer (i.e., centered at 5.6 μm with a filter width at half maximum of 0.15 μm). The sampling frequency for the two radiometers was 100 Hz. Two color cameras were used for flame and droplet imaging and a digital image acquisition system was used to acquire images every 1/30th of a second.

Prior to each test, a target atmosphere was established through partial-pressure mixing of air with a gas blend consisting of 21% O₂ and 79% CO₂, by volume. This effectively displaces atmospheric N₂ with CO₂ while holding the O₂ concentration constant at 21%. Using this approach, test atmo-

spheres ranging from 0% CO₂ to 71% CO₂ were obtained for total pressures of 1 atm, 3 atm, and 5 atm by adding the required amount of air.

The test conditions, along with the initial droplet diameter, D_0 and the average experimental burning-rate constant, K_{exp} , are presented in Table 1 for both methanol and n-heptane. Initial droplet diameters are determined from the droplet projected area while suspended in 1-g immediately prior to energizing the igniter. The volume of the suspended droplet is obtained by integrating the projected area from the backlit image and rotating this about the axis of symmetry. An effective droplet diameter is then calculated by assuming the volume of fuel is spherical in shape. The slope of the square of the instantaneous droplet diameter, $D(t)^2$, plotted against time after 0.75 seconds from ignition is used to obtain average experimental burning-rate constants.

3. Results and Discussion

Droplet regression rates were measured and used in determining the average burning-rate constants. These are compared with theoretical calculations at the various test conditions (i.e., pressure and CO₂ concentrations) for each fuel type. Flame shapes are characterized by plotting the ratio of flame diameter to droplet diameter, and representative images of the flames at 1.0 second and 4.0 seconds after ignition are presented. Finally, peak radiation measurements are presented for the broad-band radiometer at each of the ambient pressures and the ratio of the narrow-band radiometer to broad-band measurement is compared at 1 atm and 5 atm ambient pressures.

3.1 Burning Rates

Theoretical burning-rate constants, K_{cal} , for each of the test conditions presented in Table 1 were calculated using the following formula [7]:

$$K_{cal} = 8 \frac{\lambda_g}{\rho_l \cdot C_{pg}} \ln(B + 1). \quad (1)$$

The thermal conductivity, λ_g , and the specific heat, C_{pg} , of the gas mixture of the inner region between the droplet surface, r_s , and the flame, r_f , are calculated at an average temperature, \bar{T} . This temperature is given by $\bar{T} = (T_a + T_b)/2$, where, T_a is the adiabatic flame temperature and T_b is the fuel's boiling temperature at the appropriate ambient test pressure. Variations of the droplet density, ρ_l , with T_b at each test pressure were considered. The adiabatic flame temperature is obtained using the *Chemical Equilibrium with Applications* [8] ("CEA") computer code allowing for dissociation of the various equilibrium reaction species for the different pressures and different CO₂ concentrations at which the experiments were performed. The transfer number, B , defined as the ratio of energy released from the combustion reaction to the energy required to evaporate the liquid fuel, is given by the following formula when the temperature of the droplet is assumed uniform and equal to the fuel's boiling temperature, T_b , and when it is assumed that the O₂ mass fraction equals zero at the fuel surface (i.e., $Y_{o,l} = 0$) [9].

$$B = \frac{\Delta H \cdot f \cdot Y_{o,\infty} + C_{pg}(T_\infty - T_b)}{L} \quad (2)$$

Table 1: Microgravity droplet combustion tests performed at pressures of 1 atm, 3 atm, and 5 atm in 21% O₂ and ambient CO₂ concentrations ranging from 0% to 71%, by volume.

methanol			n-heptane		
CO ₂	Do (mm)	K _{exp} (mm ² /s)	CO ₂	Do (mm)	K _{exp} (mm ² /s)
P _∞ = 1 atm			P _∞ = 1 atm		
0%	1.90	0.54	0%	1.87	0.58
11%	1.81	0.54	10%	2.08	0.61
20%	1.97	0.54	10%	1.97	0.68
22%	1.96	0.54	11%	1.93	0.68
36%	1.85	0.54	16%	1.96	0.62
40%	1.91	0.50	21%	1.86	0.59
55%	1.85	0.52	31%	1.95	0.62
70%	2.03	0.52	40%	1.87	0.55
			41%	2.08	0.57
			50%	2.05	0.62
			54%	1.97	0.61
			55%	1.96	0.64
			65%	2.03	0.60
			70%	1.82	0.60
P _∞ = 3 atm			P _∞ = 3 atm		
0%	1.89	0.61	0%	1.97	0.94
21%	2.05	0.60	12%	1.87	0.90
35%	2.05	0.63	15%	2.08	0.96
50%	1.84	0.57	17%	2.02	0.91
70%	1.90	0.53	22%	1.97	0.90
			30%	1.91	0.98
			51%	1.87	1.05
			65%	1.96	0.99
			70%	2.06	0.95
			77%	1.94	0.97
P _∞ = 5 atm			P _∞ = 5 atm		
0%	2.03	0.65	0%	2.02	1.04
20%	2.24	0.60	10%	1.87	1.02
41%	2.07	0.63	31%	2.01	1.12
51%	2.14	0.59	41%	1.89	1.19
69%	1.88	0.53	60%	1.92	1.10
			70%	1.87	1.01
			71%	2.01	1.13

In the above formula, $Y_{o,\infty}$, is the ambient oxygen mass fraction, L , is the heat of vaporization of the liquid fuel, C_{pg} , is the specific heat of fuel vapor, f , is the stoichiometric fuel/oxygen mass ratio, and, ΔH , is the heat of reaction per unit mass. Values for L were obtained for the different values of T_b for each of the test pressures.

As recommended by Law and Williams [7] the thermophysical properties of the inner region's gas phase mixture were determined using only fuel vapor for the values of C_{pg} and a composition comprising a mixture of fuel vapor, reaction products, and the ambient inerts (i.e., various concentrations of CO₂ and N₂ depending on the test conditions). This can be summarized by the following expressions:

$$\lambda_g = 0.4 \lambda_f + 0.6 (\lambda_{pr+inerts}) \quad (3)$$

$$C_{pg} = C_{pf} \quad (4)$$

In Figure 1 experimental burning-rate constants for methanol are plotted against the theoretical burning-rate constants. Results show reasonably good agreement between experiment and theory with all points falling within 10% error bands, which are shown on the plot. This agreement even holds at the higher test pressures suggesting that the d^2 -law theory captures most of the physics. This is understandable because during methanol droplet combustion very little soot formation was observed and radiation effects play a minor role for initial droplet diameters below 2 mm. A similar observation was reported by Bae and Avedisian [10] for nonane droplets burning in helium/nitrogen environments. Their experimental results showed that when the helium concentrations in the ambient were increased beyond a certain level, soot formation was suppressed due to lowered flame temperatures and the burning rate followed the classical d^2 -law behavior.

In Figure 2, experimental burning-rate constants for n-heptane are plotted against theoretical burning-rate constants. Here results show a substantial increase in burning rate with ambient pressure; as much as 79% for n-heptane droplets burning in air at 5 atm compared to 1 atm. Clearly the simplified d^2 -law theory is not able to predict the increase in burning rate with pressure. At higher pressures n-heptane droplets soot profusely even at increased CO₂ concentrations leading to an increase in luminous radiation (see Figure A-2). This increased radiation could lead to heat loss from the flame zone reducing the burning rate, or, the fuel droplet could absorb an increased amount of radiant energy from the gas phase causing an increase in burning rate [11]. Earlier studies investigating the effects of initial droplet size of sooting droplets showed that an increase in sooting with initial droplet size actually decreases the burning rate. However, in this study where an increase in sooting is brought about by increasing ambient pressures, the burning rate increases with the increased sooting propensity.

This observation might lead one to conclude that an increased radiation absorption by the droplet causes this increase in burning rate. However, we have also observed that at higher pressures the flame shapes are not spherical and are highly distorted with agglomerated soot particles breaking through the flame. The soot particle dynamics induces mixing in the gas phase and causes non-spherical soot-shell motions which may also enhance the heat transfer to the droplet surface leading

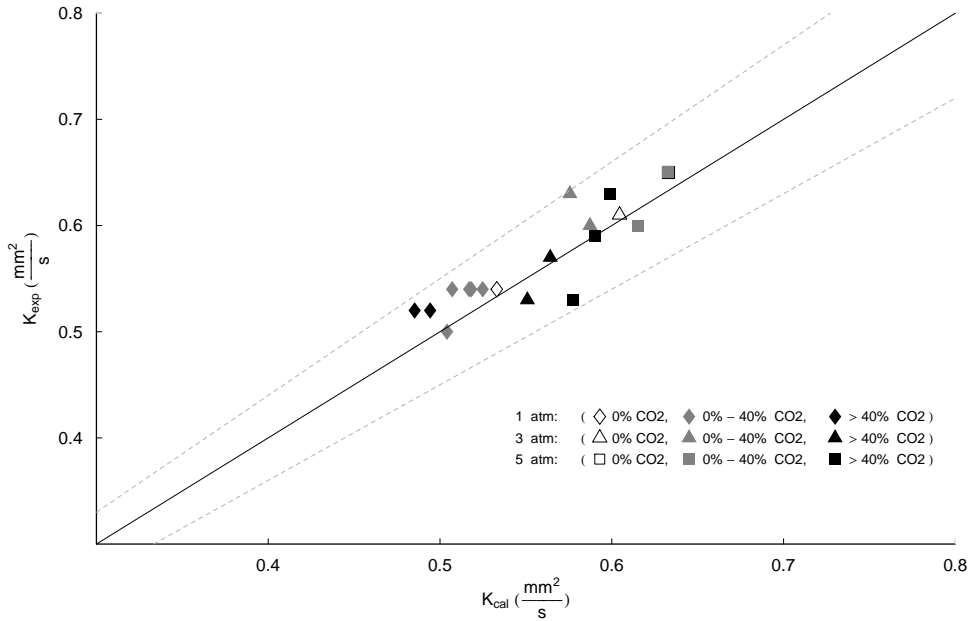


Figure 1: Experimental burning rates for methanol droplets plotted against theoretical burning rates with X_{CO_2} ranging from 0% to 70% (mole fraction), $D_o = 2.0 \text{ mm} \pm 0.20 \text{ mm}$, and ambient pressures at 1 atm, 3 atm, and 5 atm. Experimental results are within $\pm 10\%$ of the theoretical calculations as shown by the upper and lower error bands at $\pm 10\%$ of the theoretical values.

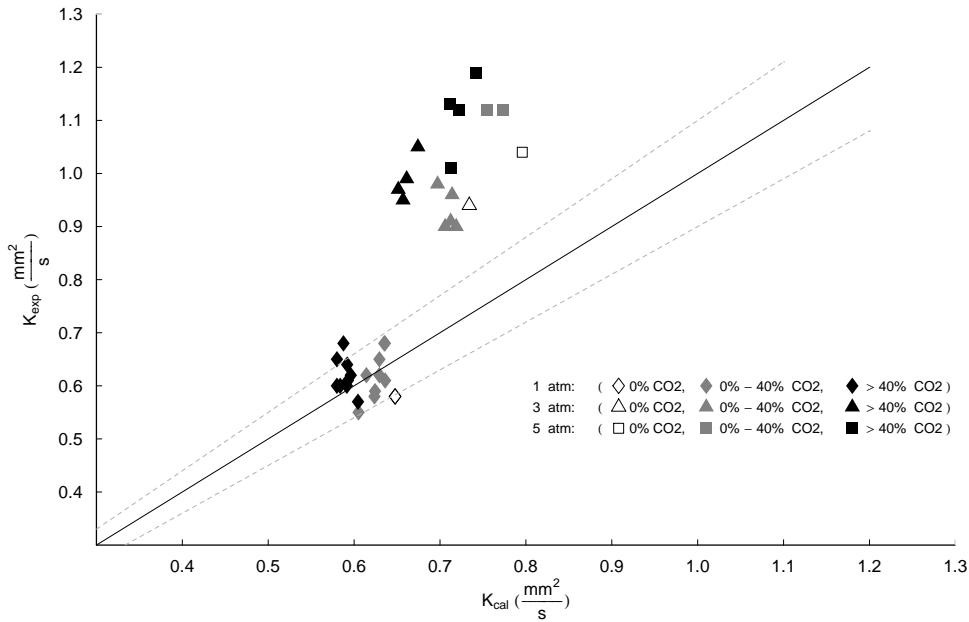


Figure 2: Experimental burning rates for n-heptane droplets plotted against theoretical burning rates with X_{CO_2} ranging from 0% to 70% (mole fraction), $D_o = 2.0 \text{ mm} \pm 0.15 \text{ mm}$, and ambient pressures at 1 atm, 3 atm, and 5 atm. Experimental results for 1 atm are within $\pm 10\%$ of theoretical calculations as shown by upper and lower error bands at $\pm 10\%$ of theoretical values.

to an increased observed burning rate. It is also interesting to note that at a given pressure the burning rate increases by a small amount with increasing concentrations of CO₂, which is a trend not seen in the methanol experiments.

3.2 Flame Shape

Flame shape is characterized by plotting the ratio of flame diameter, D_f , to the droplet diameter, d , against time and this is presented in Figure 3 for methanol droplets. At 1 atm there is a slight decrease in flame standoff ratio as the CO₂ concentration is increased. The flame standoff ratio remains almost a constant with time indicating quasi-steady burning behavior. At higher ambient pressure (see Figure 3b) the flame standoff ratio is practically independent of the CO₂ concentration and slightly lower compared to the one atmospheric cases. Furthermore, the standoff ratio initially increases with time indicating unsteady burning behavior caused by a longer droplet heating period due to increased boiling point of methanol with pressure.

Figure 4 shows the flame standoff ratio plotted against time for heptane at 1 atm and 5 atm. At 1 atm the flame standoff ratio is practically independent of CO₂ concentration and increases steadily throughout the burning period. At 5 atm the standoff ratios increase much more steeply with time and there is considerable variation with CO₂ concentration. The steeper increase is primarily due to gas phase unsteadiness inherent with heptane due to its stoichiometry. On the other hand, the variations with CO₂ can be attributed to the difficulties in exactly locating the flame front from the experiment video images. At higher pressures n-heptane soots profusely and the soot shell develops instabilities leading to a non-spherical flame appearance making it difficult to precisely locate the flame front.

Typical methanol and n-heptane flame images at different CO₂ concentrations at both 1 atm and 5 atm are shown in Figures A-1 and A-2 in the Appendix. It can be seen from these images that there is evidence of incipient sooting for methanol at 5 atm in 0% CO₂ concentration which begins to disappear as the CO₂ concentration is increased. The flame images for n-heptane at 1 atm show significant sooting in air which diminishes as CO₂ concentrations are increased. However, at 5 atm the sooting tendency, although somewhat diminished with increasing CO₂ concentrations, was still very pronounced for all ambient CO₂ concentrations.

3.3 Flame Radiation

Plots of the maximum radiant flux measured by the broad-band radiometer as a function of CO₂ concentration are shown in Figure 5 for methanol and heptane at 1 atm, 3 atm, and 5 atm. For methanol there is little variation in the maximum radiant flux with pressure and this decreases only slightly with increased CO₂. This is understandable because, as explained earlier, there is little variation in the sooting intensity with pressure for methanol and the reduction in maximum radiant output can be attributed to the reduction in flame temperature with increased CO₂. On the other hand, the overall maximum radiant output is higher for n-heptane compared to methanol and it shows a substantial increase with pressure. This is primarily due to the increased sooting of heptane droplets with pressure. The residence time, t_{res} , for fuel molecules in the region between the droplet surface and the flame varies as, $t_{res} \sim P/K^2$ [10]. For n-heptane, P/K^2 , increases

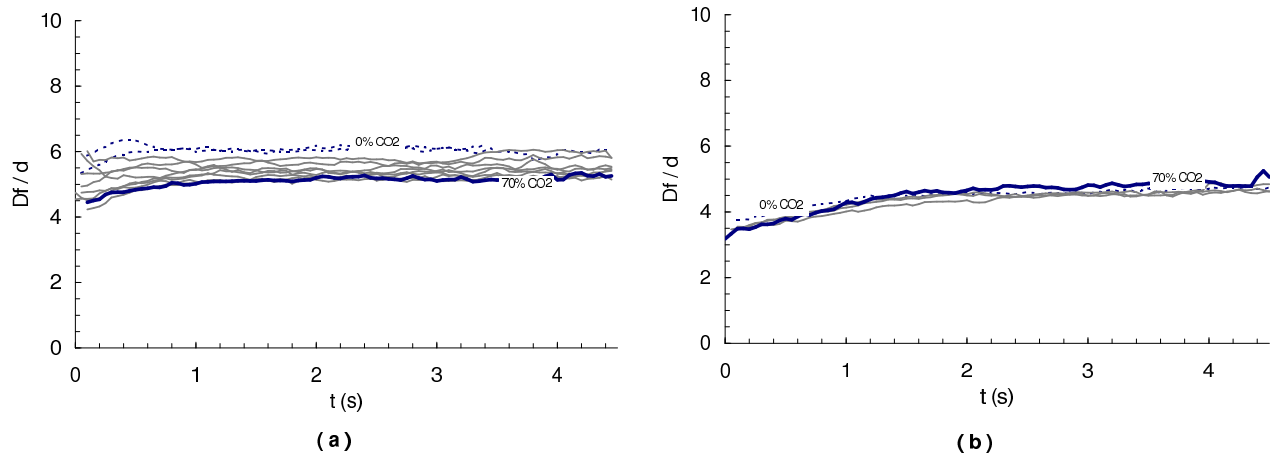


Figure 3: Ratio of flame diameter, D_f , to droplet diameter, d , for methanol flames in 1 atm (a) and 5 atm (b) with ambient X_{CO_2} mole fractions ranging from 0% (dashed blue curve) to 70% (solid blue curve).

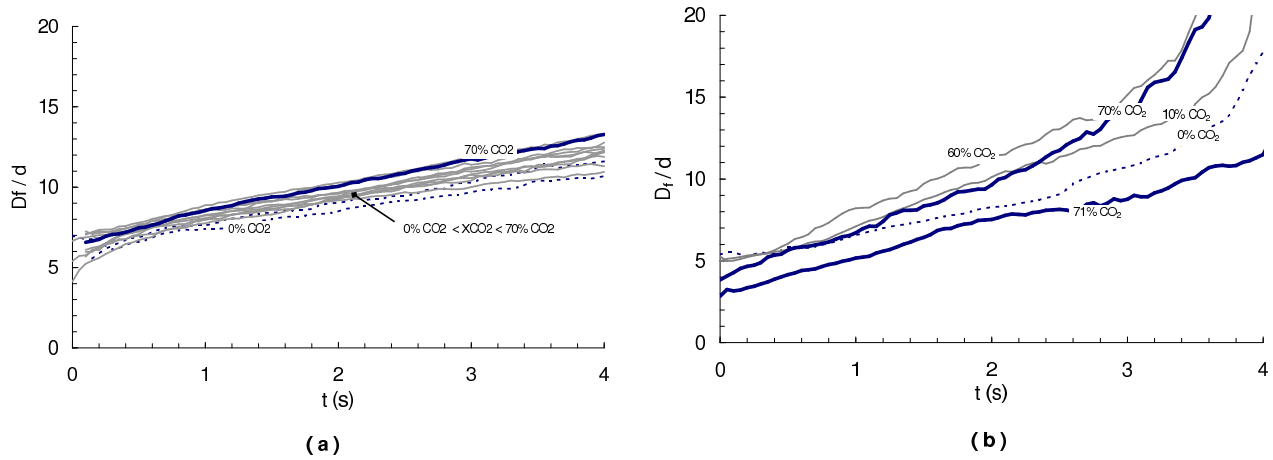


Figure 4: Ratio of flame diameter, D_f , to droplet diameter, d , for n-heptane flames in 1 atm (a) and 5 atm (b) with ambient X_{CO_2} mole fractions ranging from 0% (dashed blue curve) to 71% (solid blue curve).

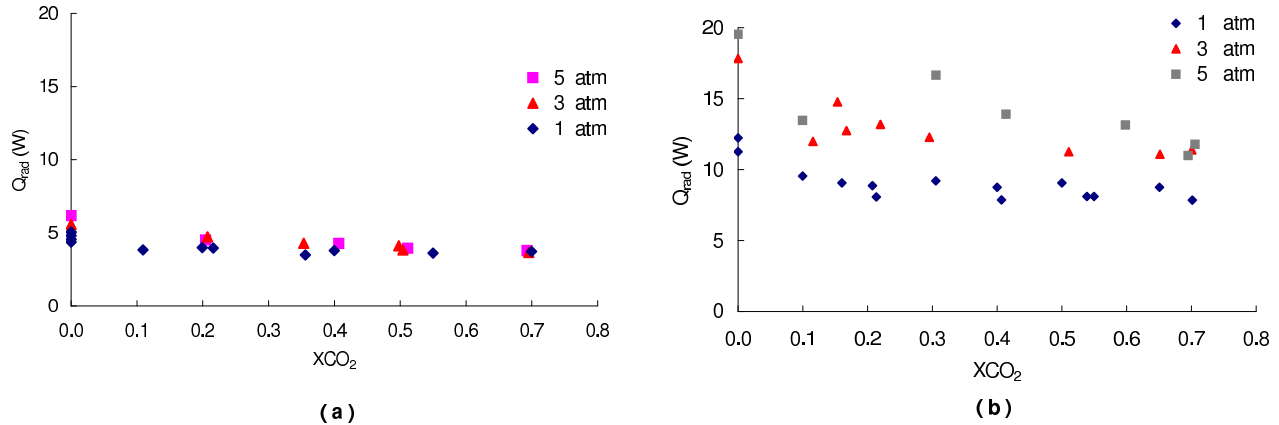


Figure 5: Maximum broad-band radiation from methanol flames (a) and n-heptane flames (b) with O_2 mole fraction constant at 21% plotted against CO_2 mole fractions ranging from 0% to 70% and at pressures of 1 atm, 3 atm, and 5 atm.

as we go from 1 atm to 5 atm pressure and consequently the soot formation and its broad-band radiation increases.

It is interesting to plot the ratio of the narrow-band radiation, which has been selectively filtered to detect radiation from the water vapor, to the broad-band radiation as a function of CO_2 concentrations. This is shown for methanol in Figure 6 and for n-heptane in Figure 7 for both 1 atm and 5 atm. Here it is seen that there is a slight increase in the ratio of narrow-band to broad-band radiation with increased CO_2 concentrations at 1 atm and a more pronounced increase in this ratio at 5 atm. For heptane droplets, where luminous radiation from soot dominates, the changes in this radiation ratio are not as substantial compared to methanol as one might expect. Further studies are needed to quantify these observations.

4. Concluding Remarks

Microgravity droplet combustion experiments were performed in elevated concentrations of CO_2 at pressures of 1.0 atm, 3.0 atm, and 5.0 atm to examine the effects of a radiatively participating suppression agent in space applications. Methanol and n-heptane droplets, with an initial diameter of 2.0 mm were used in these experiments. The ambient O_2 concentration was held constant at 21% and the CO_2 concentrations ranged from 0% to a maximum of 71%, by volume, with the balance consisting of N_2 .

Results from the methanol tests show a slight decrease in burning rates with increased CO_2 concentrations at all ambient pressures. The experimental results correlate, at all test pressures, within 10% of the theoretical results calculated using the d^2 -law formulation. This close correlation suggests that the d^2 -law captures most of the physics for methanol droplets with initial diameters of 2.0 mm burning in high ambient CO_2 concentrations at pressures ranging from 1 atm to 5 atm.

The n-heptane tests show slight increases in burning rates with increasing CO_2 concentrations at

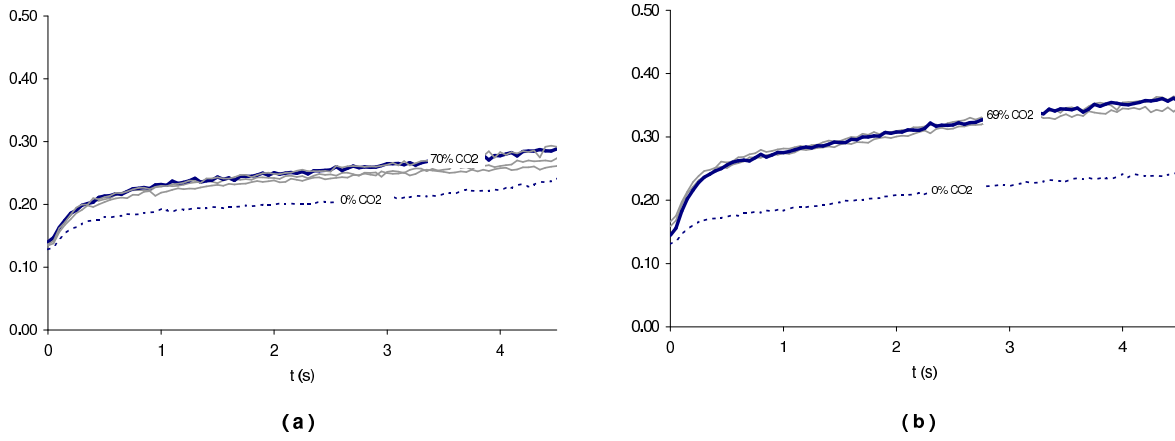


Figure 6: Ratio of narrow-band radiation to broad-band radiation for methanol flames in 1 atm (a) and 5 atm (b) with ambient concentrations of CO₂ varying from 0% to 70%.

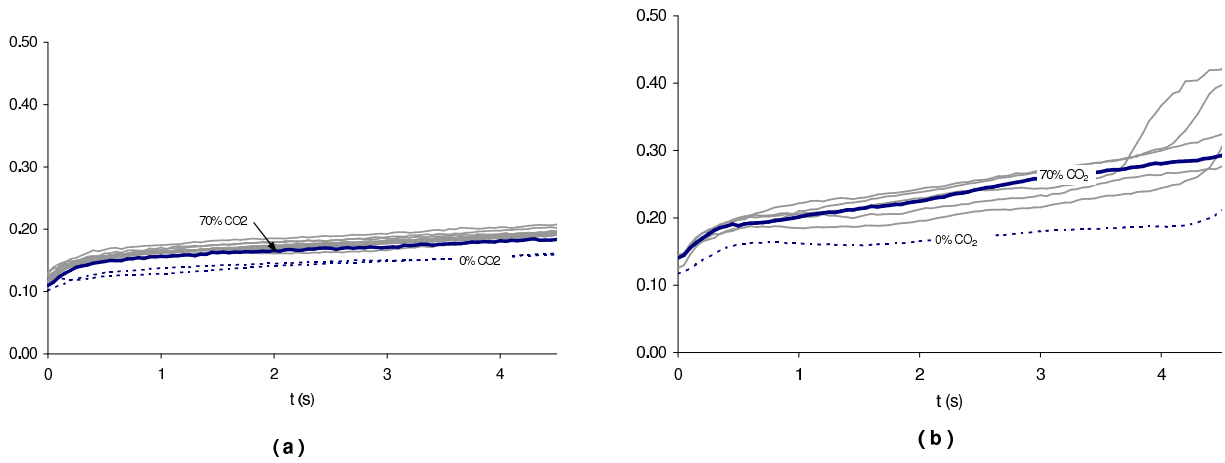


Figure 7: Ratio of narrow-band radiation to broad-band radiation for n-heptane flames in 1 atm (a) and 5 atm (b) with ambient concentrations of CO₂ varying from 0% to 70%.

each pressure level. The correlation of experimental results with theoretical calculations is within 10% for all CO₂ concentrations at 1 atm. However, a significant departure from the simplified theoretical predictions is observed at the higher test pressures of 3 atm and 5 atm. At these pressures sooting increases and this has a significant impact on the burning rates. Instabilities in the soot shell quickly develop resulting in greater mixing of the gases in the inner region and this, combined with the increased radiation from soot, increases the heat transferred to the droplet surface.

Flame shapes are characterized by plots of the ratio of flame diameter to droplet diameter. Results show little dependency with increased CO₂ concentrations at both 1 atm and 5 atm for both fuels. However, for n-heptane at 5 atm the flame standoffs show considerable variations with increasing CO₂ concentrations. This is due, in part, to the gas phase unsteadiness inherent with n-heptane flames and, in part, to the difficulty in accurately defining flame diameters due to the increased presence of soot.

The maximum radiation from the broad-band radiometer at each of the test pressures was plotted against the CO₂ concentrations. The methanol tests showed no pressure effect on the maximum radiation whereas the n-heptane tests show significant increases with pressure. When the ratio of narrow-band radiation to broad-band radiation (i.e., the ratio of water vapor emissions to broad-band emissions) is plotted against time for a range of CO₂ concentrations at 1 atm and 5 atm there is a clear increase with CO₂ concentrations in the methanol flames that is not as apparent with the n-heptane flames. The changes in the ratio of narrow-band to broad-band radiation with increased CO₂ appear to be dominated by the changes in sooting intensity as CO₂ concentrations are increased; however, this requires further study.

Acknowledgments

The authors would like to thank Eric Neumann, the facility manager of the Zero Gravity Facility, and his staff for helping with the experiments. This work was supported by the Glenn Research Center's Microgravity Fire Safety Research program.

References

- [1] L. Honda and P. D. Ronney. *Combustion Science and Technology*, 133 (1998) 267–291.
- [2] F. C. Frate, H. Bedir, C. J. Sung, and J. S. Tien. *Proceedings of the Combustion Institute*, 28 (2000) 2047–2054.
- [3] V. R. Katta, F. Takahashi, and G. T. Linteris. *Combustion and Flame*, 137 (2004) 506–522.
- [4] M. C. Hicks, N. Kaib, J. Easton, V. Nayagam, and F. A. Williams. Radiative heat loss measurements during microgravity droplet combustion in a slow convective flow. Proceedings of the 3rd Joint Meeting of the U.S. Sections of the Combustion Institute, 2003.
- [5] J. Dzik, V. Nayagam, and F. A. Williams. Ignition and combustion of n-heptane droplets in carbon dioxide enriched environments. Proceedings of the Central States Section's Spring Technical Meeting of the Combustion Institute, May 2006.
- [6] M. Ackerman, V. Nayagam, M.C. Hicks, and F.A. Williams. Combustion of droplets in steady and unsteady flows in microgravity. 43rd AIAA Aerospace Sciences Meeting, 2005.
- [7] C.K. Law and F.A. Williams. *Combustion and Flame*, 19 (1972) 393–405.

- [8] Bonnie J. McBride and Sanford Gordon. Computer program for calculations of complex chemical equilibrium compositions and application, Vol. II. Technical Report NASA RP-1311, NASA, June 1996.
- [9] Forman A. Williams. *Combustion Theory : The fundamental theory of chemically reacting flow systems*. Benjamin/Cummings, Menlo Park, CA etc., 1985.
- [10] J. H. Bae and C. T. Avedisian. *Combustion and Flame*, 145 (2006/5) 607–620.
- [11] C. T. Avedisian. *Journal of Propulsion and Power*, 16 (2000/5) 628–635.

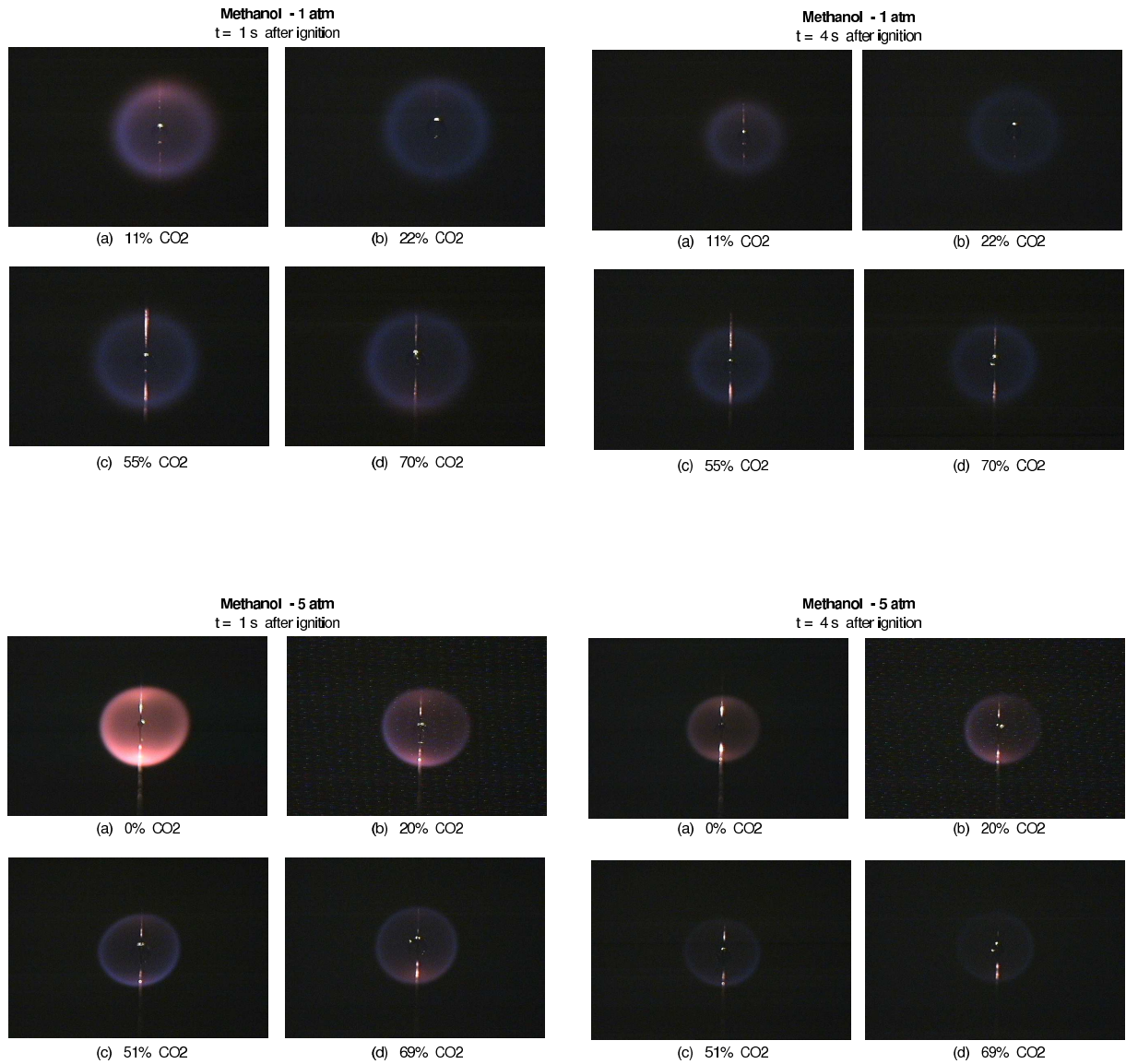


Figure A-1 Methanol droplet flames in 1 atm and 5 atm with ambient concentrations of CO₂ varying from 0% to 70% and with time after ignition at 1 second (left) and 4 seconds (right).

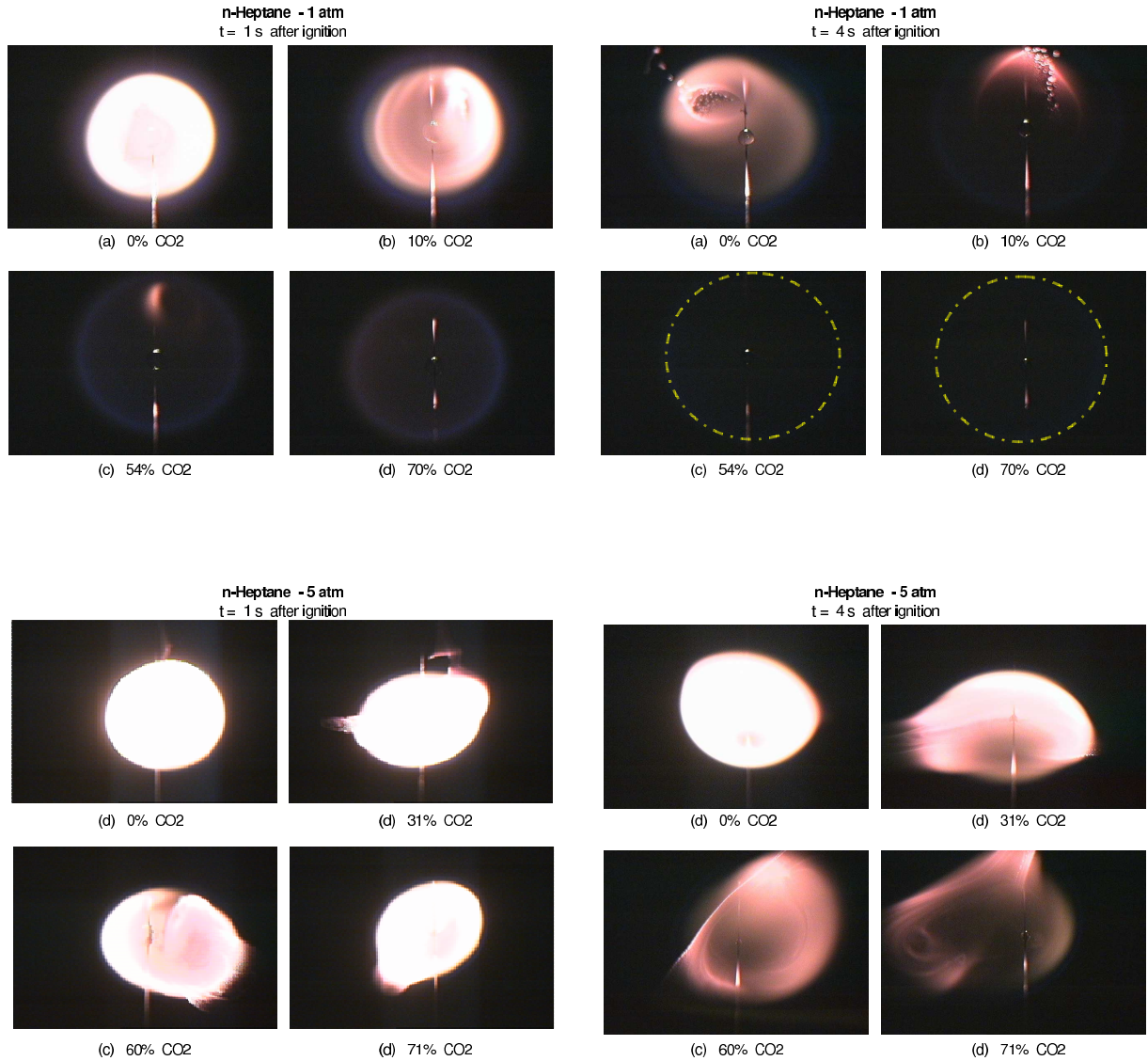


Figure A-2 Heptane droplet flames in 1 atm and 5 atm with ambient concentrations of CO₂ varying from 0% to 70% and with time after ignition at 1 second (left) and 4 seconds (right). A dashed circle is overlaid on the actual outer edge of the flame for the 1 atm tests at 54% CO₂ and 71% CO₂ at 4 seconds following ignition to highlight the positions of these extremely faint flames.